Particle-Melt Pool Interactions in Multi-Material Laser Based Directed Energy Deposition

R. Sellers*, B. Gould†, S. Wolff*

*Department of Industrial and Systems Engineering, Texas A&M University, College Station, TX 77840; †Applied Materials Division, Argonne National Laboratory, Lemont, IL 60439

Abstract

Laser based metal directed energy deposition (DED) is an additive manufacturing process that is currently on the rise in the industry. However, there is still a knowledge gap in the understanding of fundamental interactions between particles and the melt pool in the DED process and how to change the parameters to alter microstructure. This work utilized synchronized in-situ thermal and X-ray imaging to understand the anomalous behavior of molybdenum powder binding onto a Ti-6Al-4V substrate as fundamental understanding for layer-by-layer processing. Using these visual techniques, particle velocity, mass, surface energy, kinetic energy, contact area, and temperature were observed and calculated. The correlation is shown and recorded to understand the wettability of particles and why some will bounce off of the substrate while others enter the melt pool. This work will allow for the manipulation of particle-melt pool interactions in DED which will help reproduce and build better parts more efficiently.

Keywords: additive manufacturing, directed energy deposition, Ti-6Al-4V, x-ray imaging, thermal imaging, Molybdenum, surface energy

Introduction

Additive manufacturing (AM) is a process that adds material in a layer-by-layer fashion in the 3D space. The difference between regular machining and AM is the creation of complex and intricate parts, material efficiency, and reduced manual interference. Most AM processes use a powder and fuse it together with either a laser or other binding material. In directed energy deposition (DED), powder is deposited onto a substrate along with an inert gas as a laser makes a

scan and melts the two materials together. DED is great for being able to rapid prototype parts and repair components that would otherwise be too complicated to fix with traditional manufacturing [1, 2].

Metals can be used as both the substrate and as the powder, but other materials can be used during deposition, such as ceramics, biomaterials, and polymers [3]. Ti-6Al-4V (Ti64) is a widely used and studied alloy in AM due to its high melting point, light weight, strong durability, and mechanical properties [4]. Molybdenum (Mo) however, is not a common material used in AM but has promising characteristics for environments with harsh conditions such as a high melting point and corrosion resistant properties. This study focuses on the thermodynamic behavior of Mo particles binding onto a Ti64 substrate.

Many previous studies have been conducted on titanium based DED experiments. These studies have focused on looking at the mechanical, thermodynamic, and microstructural properties [1, 2, 5, 6, 7, 8]. It is important to understand these concepts and how the process affects the final product in order to alter the experiment parameters for the best possible outcome. One of the phenomena that is crucial to part manufacturing is porosity formation and control. Porosity is important because certain industries such as biomedical devices may need porosity to make parts lighter, but other applications, such as aerospace, would characterize porosity as a defect and would want to minimize porosity in order to make parts stronger [1, 7, 8, 9]. Another key characteristic of titanium components fabricated with DED and additive manufacturing is the anisotropy in properties. The studies done show how lack of melting, porosity, and uneven gas flow are defects in the manufactured part [10, 11].

This present work hopes to understand how the aforementioned defects can be avoided by looking at the binding properties of Mo and Ti64. Specifically, this work investigates if mass and velocity can be altered in order to increase the surface energy and wettability properties. If these two thermodynamic principles can be understood, then the dynamics of the melt pool, the surface roughness, and particle temperature can be predicted and controlled [11, 12]. X-Ray imaging is used to analyze the behavior of the Mo particles interacting with the Ti64 surface as well as to capture any phenomenon in the substrate as well such as melt pool boundary, porosity, the keyhole cavity, and un-melted particles.

Materials and Methodology

Material and Setup

The material used for this experiment was Ti-6Al-4V (Ti64) and Molybdenum (Mo). Ti64 alloy was used as the base of the experiment while Mo powder was deposited on top of the substrate. The operating laser had a max output of 520 W, but was cut down to 60 and 40% for certain experiments shown in Table 1.

Table 1. Experiment parameters in the lab

Experiment	Gas Pulse (ms)	Wheel Pulse (ms)	Laser Power (W)	Scan Speed (m/s)	Gas Pressure (PSI)
1	1000	0.1	208	0.1	25
2	400	0.1	312	0.1	25
3	1000	0.1	312	0.1	25

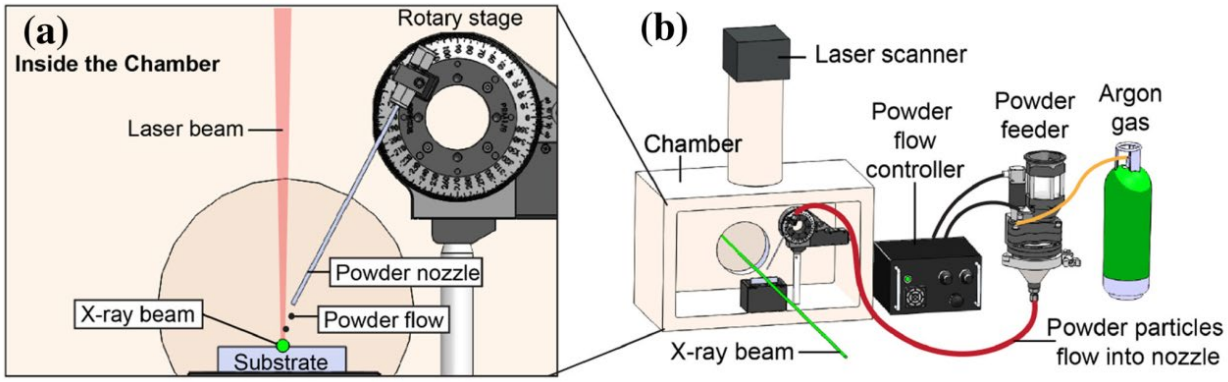

Figure 1. DED setup at Argonne National Laboratory [1]

Methodology

The three experiments presented in this work were conducted at Argonne National Laboratory. At the lab, a custom built DED was designed to run experiments with a test chamber, argon powered powder delivery control, and a laser. Specific details on the equipment and setup can be found in past work by Wolff et al. [1, 2].

Analyzing surface tension of a particle-substrate interaction requires velocity, mass, contact area, kinetic energy, temperature, and potential energy. The first observation in the experiment is the particle's velocity and how it is affected throughout its time in the sequence. In order to track particle velocity accurately and precise, an ImageJ plugin, TrackMate, was used. TrackMate

allows for the tracking of particles in the form of spots and links, which tells the user the distance from each spot placement [13]. Spots were tracked from the center of each particle from one frame to the next frame of the x-ray image sequence. After the specific particle was tracked, the data was exported to an excel sheet.

The particle displacement (μm) was then converted from micrometers to micrometers per second by multiplying by the framerate of the high-speed camera that collected X-ray images, which was 30,000 fps. This number was then converted into m/s as shown in Table 2. The frame number represents the frame from the X-ray images where the particle of interest was tracked. This means from frame 68 to frame 69, the particle of interest traveled 38.228 μm. The goal of this data is to show how much the velocity changes before and after a particle impacts the substrate. In frame 80, the particle impacts the substrate which then allows for the observation of the before and after velocity change for that specific moment.

Table 2. Example of velocity conversion from experiment 1, particle 1

Frame	**Displacement (μm)**	**Velocity ($\mu m/s$)**	**Velocity (m/s)**
68	38.845	1165350	1.16535
69	38.228	1146840	1.14684
70	39.795	1193850	1.19385
71	37.537	1126110	1.12611
72	37.926	1137780	1.13778
73	39.308	1179240	1.17924
74	38.617	1158510	1.15851
75	38.465	1153950	1.15395
76	39.999	1199970	1.19997
77	37.019	1110570	1.11057
78	40.304	1209120	1.20912
79	36.325	1089750	1.08975
80 (impact)	27.76	832800	0.8328
81	30.187	905610	0.90561
82	30.749	922470	0.92247

The angle at which the particle contacted the substrate was also measured. This was done using the built-in angle measurement tool in ImageJ. Figure 2 shows the measurement of a particle at the contact point with the substrate. The angle measured is known as the equilibrium angle, θ_E, and it used to help find the surface energy and temperature at the localized substrate surface area at particle impact. The yellow 'v' shaped lines represent the trajectory using TrackMate to help show the path and angle of the particle as it bounced off of the Ti64 substrate.

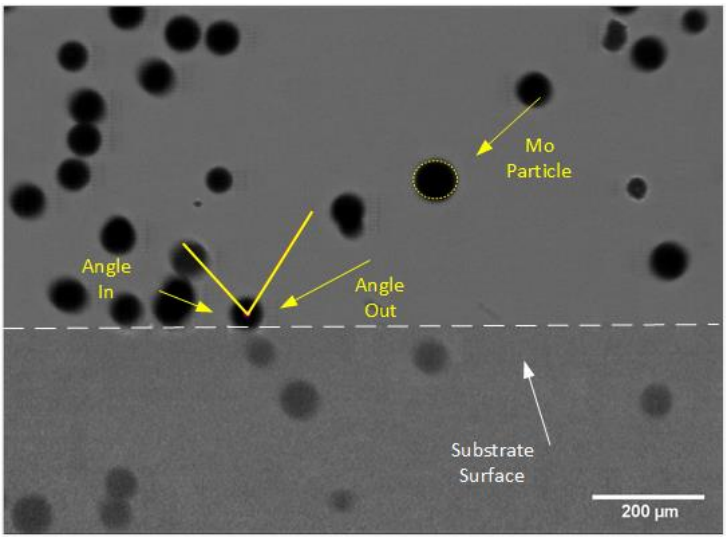

Figure 2. Measurement of the equilibrium angle of the particle deposited onto the substrate. This image was taken in the software, ImageJ, with the pixel to distance scale of 1:1.97 μm

Results and Discussion

In order to understand what properties and variables to look at, Zhou, K et. al. [4], found that the measured surface tension for Ti-6Al-4V follows a linear path represented as a trendline in Figure 3, which is shown to be 3.13×10^{-9}.

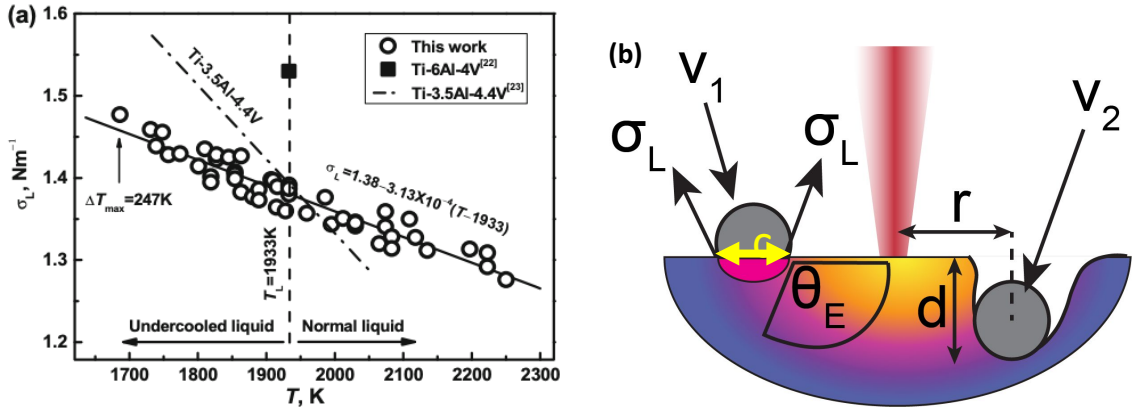

Figure 3. A) Graph of surface energy for Ti-6Al-4V to respective temperature [4], b) Graphical representation of the different variables for the calculations and how to tell which values from the table to use. σ_L represents the surface tension of Ti64, V_1 and V_2 represent the particle velocity before and after, respectively, θ_E is the equilibrium angle, r is the distance from impact to laser, c and d are the diameters of the impact area and the particle, respectively

Particle Angle

The equilibrium angle for each particle in the respective experiment can be found in Table 4. The theory of wettability is the measurement of a how well a liquid interacts with either another liquid or a solid [5]. Equilibrium angles play a key role in wettability because depending on how large or how small the angle is, the droplet will interact differently with the surface. In the experiments performed, solid Mo particles were deposited onto a solid or liquid substrate, where usually wettability is measured for liquids or droplets deposited onto hard surfaces. Since it is harder to deposit single droplets of liquid Mo to measure, some of the equations and applications had to change slightly due to the different circumstances to account for the two solids. For these experiment purposes, if the particle entered the liquid melt pool, the equations would use an equilibrium angle less than 90° and if the particle bounced off the solid substrate surface, the angle would be greater than 90°.

Particle Velocity

With the data recorded in Table 3 and graphically represented in Figure 4, it is shown that as the particle mass increases, the velocity decreases. This decrease is represented from the trendline shown on the graph, which gives a rough estimate for the claim of slower velocity due to larger particle mass. More data points would help justify the theory and to fill the graph for more representation. This graph however is specifically the V_{in} which means that it only shows how fast the particles were moving before they contacted the substrate. This was done to show correlation between velocity and mass, since different factors such as the laser, molten liquid, and hitting other particles can affect a particle after contact. Figure 5 shows the velocity before and after surface contact for the four particles recorded in experiment 1. This graph helps visualize the change in velocity of the two particles that entered the melt pool and the two that bounced off.

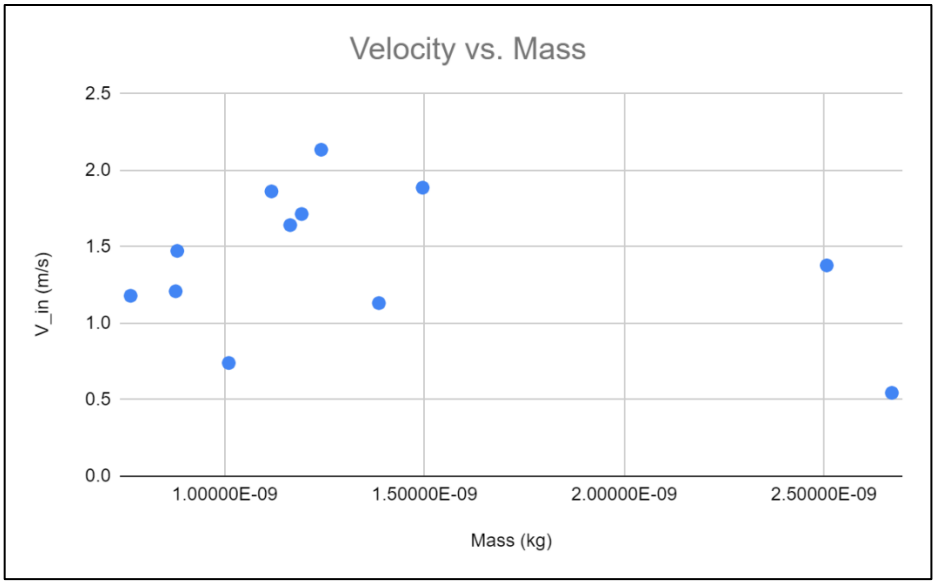

Figure 4. Graph of V_{in} for all particles and experiments with the included trendline. This was made using Excel's graph function

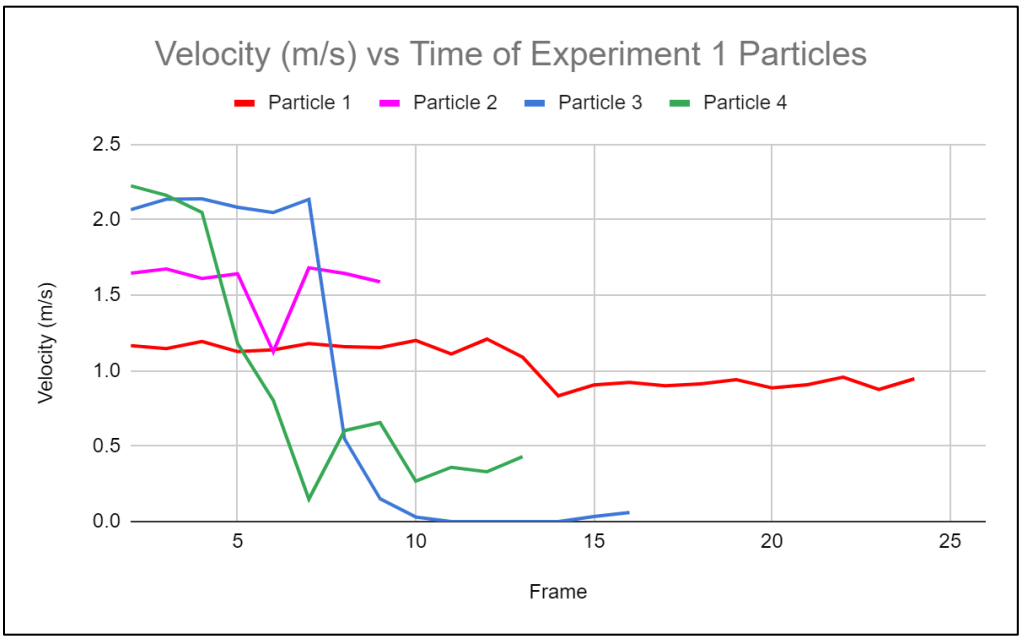

Figure 5. Graph of velocity and time for only experiment 1. The frames for the x-axis are just for reference and not specific to the actual frame/time from the x-ray sequence that the particle was captured in. This is to reference how long each frame lasts, which is about 0.041 seconds per frame.

Surface Tension

After discovering the velocity of the observed particles, the surface tension of the substrate can be found along with the temperature of the area of impact near the particle. The first step is finding the mass of the tracked Molybdenum particle. Mass is calculated with Eq. 1, which is the density of Ti64 multiplied by the volume of the particle and 2.3. This is the base equation for mass that includes volume and density. The 2.3 multiplier is because Mo is 2.3 times denser than Ti64.

$$mass\ (m) = 2314 \times (diameter)^3 \times 2.3 \quad (1)$$

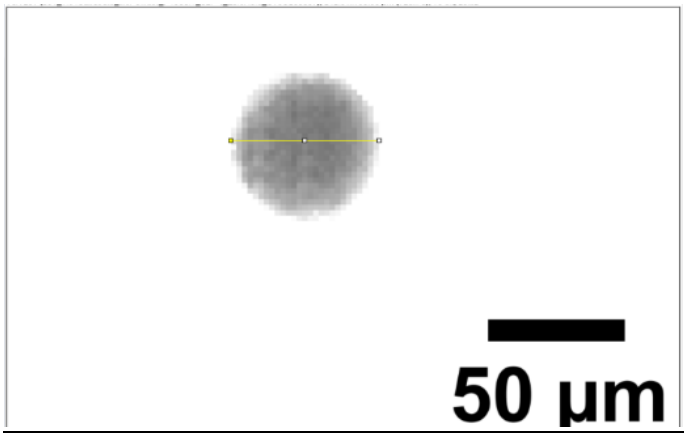

Figure 6. Image showing the measurement of a Molybdenum particle using ImageJ's line tool, with the pixel to distance scale of 1:1.97 μm

As shown in Table 3, the particles each had similar masses of around 10^{-9} and 10^{-10} kg, which indicates that there were no outliers or drastic changes in particle diameter. The next variable to calculate was c_{area}, the contact area the particle had with the surface of the substrate. Using Eq. 2, the contact area could be calculated using c, which was the diameter in meters of the portion of particle that was in contact with the substrate in Fig 7. A list of different contact areas can be found in Table 3. One of the important reasons for understanding contact area is that it plays a key role in particle wetting. When the particle has an increased contact area with the surface, the probability of it entering the melt pool increases.

$$c_{area} = \pi \left(\frac{c}{2}\right)^2 \quad (2)$$

An issue with recording the contact area through x-ray images is that the point of reference depends on the framerate of the camera. This means that if the particle could not be captured at the exact moment of contact, it is assumed that c is very small, or 10^{-6} m, which makes the

c_{area} small as well. Contact area measurement is critical in the calculations as it dictates how large or small the T value is.

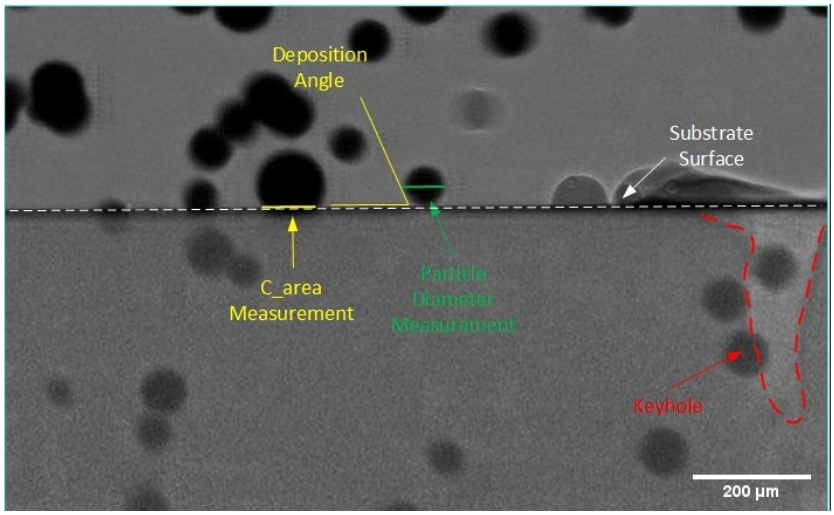

Figure 7. Image showing the measurement of the diameter of the particle that is in contact with the surface of the substrate. This is using *ImageJ's* line tool for accuracy and measurement with the pixel to distance scale of 1:1.97 μm

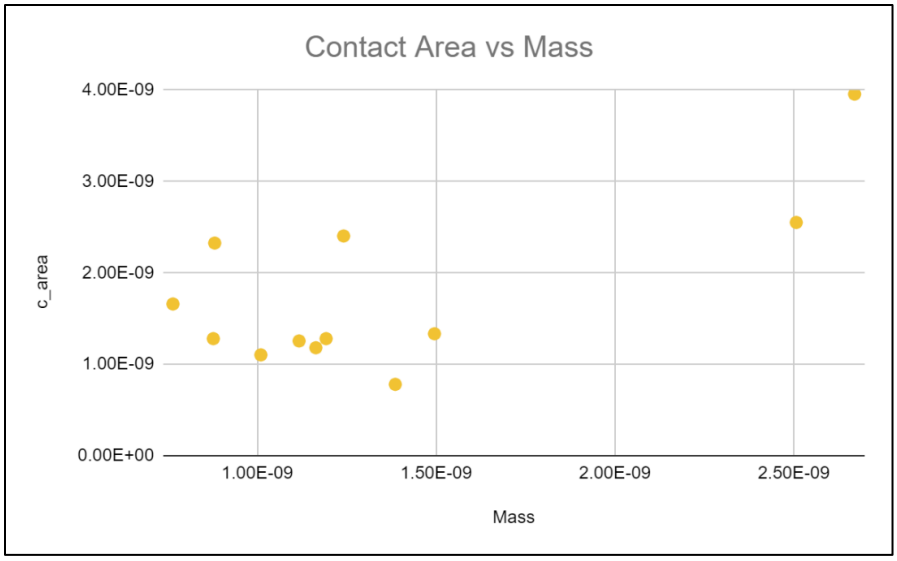

Figure 8. Graph showing the relationship of contact area and mass

The kinetic energy of the particle can be found using the two equations, Eq. 3 and Eq. 4. The variables V_{in} and V_{out} are only used when the particle bounces off of the substrate. This constraint also applies to Eq. 5 and Eq 6. The average kinetic energy was found to be 1.118×10^{-9} J, 1.052×10^{-9} J, 1.328×10^{-9} J for experiments 1, 2, and 3, respectively.

$$KE = \frac{1}{2}mv^2 \quad (3)$$

$$KE = \frac{1}{2}m(v_{in}^2 - v_{out}^2) \quad (4)$$

Surface tension requires a localized temperature at that point to be known. In order to calculate this number, Eq. 5 and Eq. 6 are used**.** These equations account for the particle bouncing off of the substrate and the particle entering the melt pool, respectively. If the particle bounces off of the substrate, T should theoretically be less than $\sim 1600°C$. If the particle enters the melt pool, then the value should be somewhere between $1600 - 3000°C$, which is the melting point range of Ti64. Anything higher than $\sim 3000°C$ should be the boiling point of Ti64. The final calculation needed is Eq. 7, which is the surface energy of the Ti64 alloy. This equation uses the localized T value calculated previously in order to find the surface tension at the particular point. The theory of wettability says that if the kinetic energy is greater than the surface tension, then the particle will enter the melt pool. A list of T and σ_L values can be found in Table 3 for each particle tracked in the experiments. Surface tension varies with differing surface properties such as viscosity, rigidity, or surface finish [4].

$$T = 3195 \times \left(1.38 - \frac{m(v_{in}^2 - v_{out}^2)}{2c_{area}(1+\cos(\theta_E))}\right) + 1933 \quad (5)$$

$$T = 3195 \times \left(1.38 - \frac{mv^2}{2c_{area}(1+\cos(\theta_E))}\right) + 1933 \quad (6)$$

$$\sigma_L = c_{area} \times \left(1.38 - 0.000313(T - 1933)\right) \times (1 + \cos(\theta_E)) \quad (7)$$

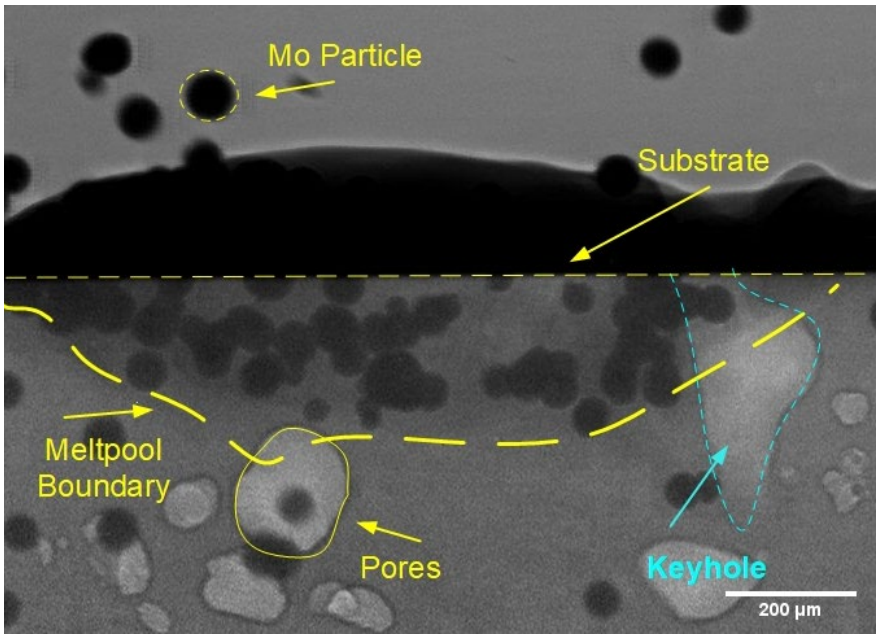

Figure 9. Image of Experiment 3 mid process that captures the different occurrences such as the key-hole, powder deposition, porosity, melt pool, and molten substrate. Analyzed in ImageJ and annotated in Microsoft Visio.

Table 3. Data from three experiments and their respective particle numbers

Experiment	Particle Number	Mass (kg)	$c_{area}(m^2)$	$KE\ (m/s^2)$	$T\ (°C)$	σ_L	V_{in}	V_{out}
Experiment 1	Particle 1	8.77E-10	1.28E-09	2.8154244E-10	1,411.97	2.8154348E-10	1.20912	0.90561
	Particle 2	1.16E-09	1.18E-09	8.3188002E-10	1,910.15	8.3188017E-10	1.64208	1.12566
	Particle 3	1.24E-09	2.40E-09	2.8297277E-09	4,197.04	2.8296232E-09	2.13498	
	Particle 4	7.64E-10	1.66E-09	5.3199920E-10	5,747.59	5.3187972E-10	1.17978	
Experiment 2	Particle 1	1.01E-09	1.10E-09	1.39E-11	5,374.98	2.05E-10	0.74052	0.37842
	Particle 2	1.12E-09	1.26E-09	1.9377969E-09	3,534.98	1.9377582E-09	1.86258	
	Particle 3	2.67E-09	3.96E-09	3.9639170E-10	6,142.01	3.9609987E-10	0.54489	
	Particle 4	2.51E-09	2.55E-09	1.2022050E-09	1,923.38	1.2022051E-09	1.37844	0.97011
Experiment 3	Particle 1	1.19E-09	1.28E-09	5.9275445E-10	1,663.53	5.9275565E-10	1.71453	1.39485
	Particle 2	1.39E-09	7.80E-10	6.0586086E-11	1,788.73	6.0586153E-11	1.1319	1.0926
	Particle 3	1.50E-09	1.33E-09	2.6621482E-09	2,460.04	2.6621355E-09	1.88679	
	Particle 4	8.81E-10	2.33E-09	9.5607459E-10	5,520.30	9.5592852E-10	1.47312	

Table 4: Data from the twelve particles and their respective equilibrium angles

Data Table	Particle Number	Angle In	Angle Out
sExperiment 1	Particle 1	51.34	149.04
	Particle 2	60.02	119.49
	Particle 3	41.10	
	Particle 4	43.73	
Experiment 2	Particle 1	62.06	112.76
	Particle 2	48.12	
	Particle 3	53.13	
	Particle 4	36.09	131.25
Experiment 3	Particle 1	49.28	133.15
	Particle 2	42.52	161.00
	Particle 3	50.01	
	Particle 4	53.27	

Conclusions

In this study, thermodynamic principles were analyzed and calculated for molybdenum powder deposited onto a Ti64 substrate using the DED additive manufacturing process. Although the results produced are not abundant, the process and theory prove promising and will allow for others to understand why these principles are occurring in DED experiments. It was found that the angle of particle 1 in Figure 2 increased by 190% as it bounced off. This helps understand how the equilibrium angle is altered when a particle bounces off of the substrate rather than entering the melt pool. From Figure 4, it is shown that as the particle's mass increases, the velocity decreases. This leads to an increase in odds that the particle will enter the melt pool instead of bouncing off at slower speeds. Table 3 shows that with the twelve particles measured, there was no correlation between entering the melt pool and the particle's velocity. The V_{in} values ranged from 0.5 to 2.1 meters per second which shows that the velocity can vary over a long span and does not have to follow a specific trend. Particle deposition angles can be altered to increase the chance of powder absorbing into the melt pool, as shown from the measured angles in Table 4.

From these experiments, it can be concluded that increasing the particle mass will increase the contact area which will increase the chance of particle wetting. The trend shown in Figure 8 proves how changing these parameters can affect wettability. Of the six particles that entered the melt pool, the calculated localized temperature at the melt pool surface ranged from 2100 to 6100°C. From the six that bounced off of the melt pool, the temperatures ranged from 1400 to 1900°C, with the occasional temp that was outside of that range. These values follow the melting point of Ti64 and prove that powder has a higher chance of injecting into melt pool when the localized temperature is greater than the melting point. Powder deposition can be controlled to release powder at the optimal time after the laser has developed the melt pool in order to increase the binding of powder and substrate as well.

More work is needed to be done in order to understand particle interactions with the melt pool. This study does not account for un-melted particles, porosity, keyholes, and other melt pool characteristics that can affect the wettability of deposited powder. Studies can be done of the other phenomena occurring in the melt pool.

Acknowledgement

The authors would like to Tao Sun, Niranjan Parab, Kamel Fezzaa, and Alex Deriy at the beamline. This research used resources of the Advanced Photon Source, a U.S. Department of Energy (DOE) Office of Science User Facility operated for the DOE Office of Science by Argonne National Laboratory (ANL) under Contract No. DE-AC02-06CH11357 and support through Laboratory Directed Research and Development (LDRD) funding from ANL under the same contract.

Reference

[1] Wolff, Sarah J., Samantha Webster, Niranjan D. Parab, Benjamin Aronson, Benjamin Gould, Aaron Greco, and Tao Sun. "In-Situ Observations of Directed Energy Deposition Additive Manufacturing Using High-Speed X-Ray Imaging." JOM 73, no. 1 (2020): 189–200. https://doi.org/10.1007/s11837-020-04469-x.

[2] Wang, Hui, et al. "High-Speed Synchrotron X-Ray Imaging of Directed Energy Deposition of Titanium: Effects of Processing Parameters on the Formation of Entrapped-Gas Pores." *Procedia Manufacturing*, Elsevier, 8 July 2021, www.sciencedirect. com/science/article/pii/ S2351978921000202.

[3] Sarkar, Montajar, et al. "Surface, Mechanical and Shape Memory Properties of Biodegradable Polymers and Their Applications." *Reference Module in Materials Science and Materials Engineering*, Elsevier, 15 Sept. 2020, www.sciencedirect.com/science/article/pii/B978012820352100050X?via%3Dihub.

[4] Zhou, K., & Wei, B. (2016). Determination of the thermophysical properties of liquid and solid Ti–6Al–4V alloy. *Applied Physics A, 122*(3), 248.

[5] Haley, James C., et al. "Modelling Particle Impact on the Melt Pool and Wettability Effects in Laser Directed Energy Deposition Additive Manufacturing." *Materials Science and Engineering: A*, Elsevier, 20 June 2019, www.sciencedirect.com/science/article/pii/S092150931930838X?via%3Dihub.

[6] Saboori A, Gallo D, Biamino S, Fino P, Lombardi M. An Overview of Additive Manufacturing of Titanium Components by Directed Energy Deposition: Microstructure and Mechanical Properties. *Applied Sciences*. 2017; 7(9):883. https://doi.org/10.3390/app7090883

[7] Heigel, J. C., Michaleris, P., & Reutzel, E. W. (2015). Thermo-mechanical model development and validation of directed energy deposition additive manufacturing of Ti-6Al-4V. *Additive Manufacturing*, *5*, 9–19. https://doi.org/10.1016/j.addma.2014.10.003

[8] Kistler, N. A., Corbin, D. J., Nassar, A. R., Reutzel, E. W., & Beese, A. M. (2019). Effect of processing conditions on the microstructure, porosity, and mechanical properties of Ti-6Al-4V repair fabricated by directed energy deposition. *Journal of Materials Processing Technology*, *264*, 172–181. https://doi.org/10.1016/j.jmatprotec.2018.08.041

[9] Carroll, B. E., Palmer, T. A., & Beese, A. M. (2015). Anisotropic tensile behavior of Ti-6Al-4V components fabricated with directed energy deposition additive manufacturing. Acta Materialia, 87, 309–320. https://doi.org/10.1016/j.actamat.2014.12.054

[10] Wolff, S., Lee, T., Faierson, E., Ehmann, K., & Cao, J. (2016). Anisotropic properties of directed energy deposition (DED)-processed Ti–6Al–4V. *Journal of Manufacturing Processes*, *24*, 397–405. https://doi.org/10.1016/j.jmapro.2016.06.020

[11] Fateri, M., Pitikaris, S. & Sperl, M. Investigation on Wetting and Melting Behavior of Lunar Regolith Simulant for Additive Manufacturing Application. *Microgravity Sci. Technol.* **31,** 161–167 (2019). https://doi.org/10.1007/s12217-019-9674-5

[12] Haley, J. C., Schoenung, J. M., & Lavernia, E. J. (2019). Modelling particle impact on the melt pool and wettability effects in laser directed energy deposition additive manufacturing. *Materials Science and Engineering A*, *761*. https://doi.org/10.1016/j.msea.2019.138052

[13] Tinevez JY, Perry N, Schindelin J, Hoopes GM, Reynolds GD, Laplantine E, Bednarek SY, Shorte SL, Eliceiri KW. TrackMate: An open and extensible platform for single-particle tracking. Methods. 2017 Feb 15;115:80-90. doi: 10.1016/j.ymeth.2016.09.016. Epub 2016 Oct 3. PMID: 27713081.